Photorefractive surface nonlinearly chirped waveguide arrays

Pengfei Qi,[1,2] Tianrun Feng,[1] Sainan Wang,[1] Rong Han,[1] Zhijian Hu,[1,3] Tianhao Zhang,[1,*] Jianguo Tian,[1] and Jingjun Xu[1]

[1]*Photonics Research Center, School of Physics, The MOE Key Lab of Weak-Light Nonlinear Photonics, and Tianjin Key Lab of Photonics Materials and Technology for Information Science, Nankai University, Tianjin 300071, China*

[2]*Institute of Modern Optics, Nankai University, Key Laboratory of Optical Information Science and Technology, Ministry of Education, Tianjin 300071, China*

[3]*CAS Key Laboratory of Standardization and Measurement for Nanotechnology, National Center for Nanoscience and Technology, Beijing 100190, China*

(Received 28 January 2016; revised manuscript received 2 March 2016; published 17 May 2016)

We report an alternate type of nonlinear waveguides, photorefractive surface nonlinearly chirped waveguide arrays, which can be directly induced by photorefractive surface waves in virtue of diffusion and drift nonlinearities. The amplitude of such nonlinearly chirped waveguide arrays has an apodized envelope owing to the diffusion nonlinearity. The refractive-index change of the apodized tails converges to a nonzero value which can be handily adjusted by an external electric field. Moreover, the chirp parameters such as amplitude, sign (positive or negative), and initial position can be conveniently adjusted by an external electric field, background illumination, incident beam, etc. Then the guided-wave properties of this type of waveguide arrays are analyzed by using the transfer matrix method. Owing to the flexible tail and the nonlinear chirp, the dispersion curves of the index-guided modes can be tailored by an external electric field and the dispersion curves of ordinary and extraordinary Bragg guided modes couple, intertwine, and anticross with each other. Meanwhile, there is a clear "competition" in the coupling hybrid mode near anticrossing.

DOI: 10.1103/PhysRevA.93.053822

I. INTRODUCTION

The ability to mold the flow of light in photonic periodic structures is a fundamental issue of scientific and practical importance [1]. Optical waveguide arrays have attracted considerable attention for their abundant physics and potential engineering applications [2]. Among different approaches to fabricate waveguide lattices, by the electro-optic properties of photorefractive crystals such as high nonlinearity, reconfigurability and tunability at very low power levels, optical induction has received more attention in past years. In 2002, Efremidis *et al.* theoretically suggested a new method of creating lattices using optical induction [3]. Subsequently, Fleischer *et al.* demonstrated the new method and reported a waveguide array and a two-dimensional (2D) square photonic lattice in SBN:75 [4,5]. In 2006, Freedman *et al.* induced a 2D photonic quasicrystal in SBN:75 [6]. In 2007, Peleg *et al.* induced a honeycomb lattice in SBN:75 [7]. In 2010, a three-dimensional (3D) photonic quasicrystal was realized in SBN:Ce by Xavier *et al.* [8]. These waveguide lattices offer tunable platforms for studying discrete light behaviors and emulating the intriguing phenomena in quantum systems [1,9]. It worth noting that the special defects and modulations of waveguide arrays have vast potential applications in optimizing the beam dynamics performance such as improving beam steering resolution, enhancing the soliton mobility, and tailoring diffraction properties [10–12]. However, introducing expected defects and modulations handily is still a major problem.

Photorefractive surface waves (PR SWs), taking advantage of the balance between the reflection from the surface and the self-deflection induced by nonlocal nonlinearity, can propagate along the surface of a nonlinear medium without diffraction [13]. Besides enhancing surface second harmonic generation and surface Raman scattering and exciting long-range surface plasmon *et al.* [14–16], PR SWs can be applied to inducing surface modulated waveguide arrays. In 2015 we suggested a unique apodized waveguide array (AWGA), which is directly induced by photorefractive surface waves. There were lots of intriguing phenomena such as the anticrossings between the dispersion curves of index-guided modes (IGMs) and Bragg-guided modes (BGMs), the extraordinary BGMs constituted by the splice of IGMs and BGMs [17].

At the same time, we also noted that the frequency of photorefractive surface apodized waveguide arrays (PR SAWGAs) can be tuned conveniently, in that the frequency of PR SWs can be adjusted by an external electric field, background illumination, etc. [18]. Another type of waveguides, nonlinearly chirped waveguide arrays, can be handily fabricated by utilizing PR SWs. The chirp is an optimization technology, which is as important as the apodization in waveguide grating. What is more, the chirped or/and apodized waveguide arrays have also been extensively applied in soliton controlling, diffraction management, quasi-phase-matched and optical diode, etc. [19–25]. Undoubtedly, the amplitude or/and frequency modulation of such interesting waveguide arrays will provide opportunities for various applications.

In this paper we report a different type of waveguide arrays induced by PR SWs in virtue of diffusion and drift nonlinearities. Both amplitude and local spatial frequency of such waveguide arrays can be modulated, and the refractive-index change Δn of the apodized tail converges to a nonzero value which can be handily adjusted by an external electric field. In consequence, it can be recognized as a photorefractive surface nonlinearly chirped waveguide arrays (PR SNCWGAs) with apodized envelopes. Meanwhile, we find that the chirp parameters such as amplitude, sign (positive or negative),

*Corresponding author: zhangth@nankai.edu.cn

and initial position can be adjusted conveniently. Owing to the nonlinear chirp and flexible tail of such waveguide arrays, we find lots of interesting phenomena besides the guided wave properties in AWGAs, such as the dispersion relation of IGMs can be tailored by an external electric field and the anticrossing between the ordinary and extraordinary BGMs.

II. THE INDUCTION OF NONLINEARLY CHIRPED WAVEGUIDE ARRAYS

A. Theoretical model

Considering a slit e-polarized laser beam (transverse extent of the beam along the y axis greatly exceeds that along the x axis) propagating along the interface between air and a PR crystal (PRC), with optical c axis oriented along the x axis, as shown in Fig. 1. The complex amplitude $E(x,z)$ satisfies the nonlinear scalar wave equation

$$\nabla^2 E(x,z) + k^2 E(x,z) = 0. \tag{1}$$

In the air ($x < 0$), $k = k_0 n_0 = 2\pi/\lambda_0$, $n_0 = 1$, and λ_0 is the wavelength in vacuum. In a PRC ($x > 0$), $k = k_0(n + \Delta n)$, n is the refractive index of an e-polarized beam in the PRC, Δn is the refractive-index change induced by nonlinearity, $(n + \Delta n)^2 = n^2 - n^4 r_{\text{eff}} E_{\text{sc}}$, $r_{\text{eff}} = r_{33}$ is the effective electro-optical coefficient, and E_{sc} is the space-charge field. With an o-polarized coherent uniform background illumination and an applied external electric field, E_{sc} can be written as

$$E_{\text{sc}}(x) = \frac{k_B T}{q}\frac{d}{dx}\ln[I'(x)+1] + E_0\frac{I'_\infty + 1}{I'(x)+1}, \tag{2}$$

where k_B is Boltzmann constant, T is the temperature, q is the charge of carriers (negative for the electrons and positive for the holes), and $E_0 = E_{\text{sc}}(x \to \infty)$ is the applied external electric field. $I'(x) = I(x)/(I_b + I_d)$ is the normalized intensity of light beam, $I(x)$ is the light intensity of the PR surface waves, I_b is the intensity of the background illumination, I_d is the equivalent dark irradiance, and $I'_\infty = I'(x \to \infty) = 0$ for bright surface waves. The first and the second terms on the right side of Eq. (2) describe the effects of the diffusion and drift components of PR nonlinearity, respectively.

We look for the stationary surface wave solution as $E(x,z) = A'(x)(I_b + I_d)^{1/2}\exp(i\beta z)$, where β is the propagating constant and $A'(x) = I'(x)^{1/2}$ is the normalized real amplitude of PR SWs. Then Eq. (1) can be rewritten as

$$\frac{d^2A'(x)}{dx^2} - \gamma\frac{A'^2(x)}{A'^2(x)+1}\frac{dA'(x)}{dx} - \frac{aA'(x)}{A'^2(x)+1} + gA'(x) = 0, \tag{3}$$

where $\gamma = 2k_0^2 n^4 r_{\text{eff}} k_B T/q$, $a = k_0^2 n^4 r_{\text{eff}} E_0$, and $g = k_0^2 n^2 - \beta^2$.

Obviously Eq. (3) is a nonlinear damped oscillator equation, where the second term, the third term, and the fourth term on the left side of Eq. (3) can be regarded as the damping force, the external force, and the restoring force, respectively. The effective restoring force F and the local spatial frequency $K(x)$ of PR SWs can be written as

$$F(x) = \frac{(a-g) - gA'^2(x)}{A'^2(x)+1}A'(x), \tag{4}$$

$$K(x) = \sqrt{g - \frac{a}{A'^2(x)+1} - \frac{\gamma^2 A'^4(x)}{4[A'^2(x)+1]^2}}. \tag{5}$$

According to $(n + \Delta n)^2 = n^2 - n^4 r_{\text{eff}} E_{\text{sc}}$, the refractive-index change of the waveguide induced by PR SWs can be written as

$$\Delta n = -\frac{1}{2}n^3 r_{\text{eff}}\left[\frac{k_B T}{q}\frac{dI'(x)}{[I'(x)+1]dx} + E_0\frac{1}{I'(x)+1}\right]. \tag{6}$$

B. Simulation and discussion

Taking SBN:75 as a sample, based on Eq. (3) and continuity boundary conditions, the surface waves can be numerically found by the Runge-Kutta method, the parameters used in the calculation are $\lambda = 532\,\text{nm}$, $n = 2.3117$, $r_{\text{eff}} = 1340\times10^{-12}\,\text{m/V}$, $q = -1.6\times10^{-19}\,\text{C}$, $k_B = 1.38\times10^{-23}\,\text{J/K}$, $T = 300\,\text{K}$, and $\beta = 2.730118\times10^7\,\text{m}^{-1}$.

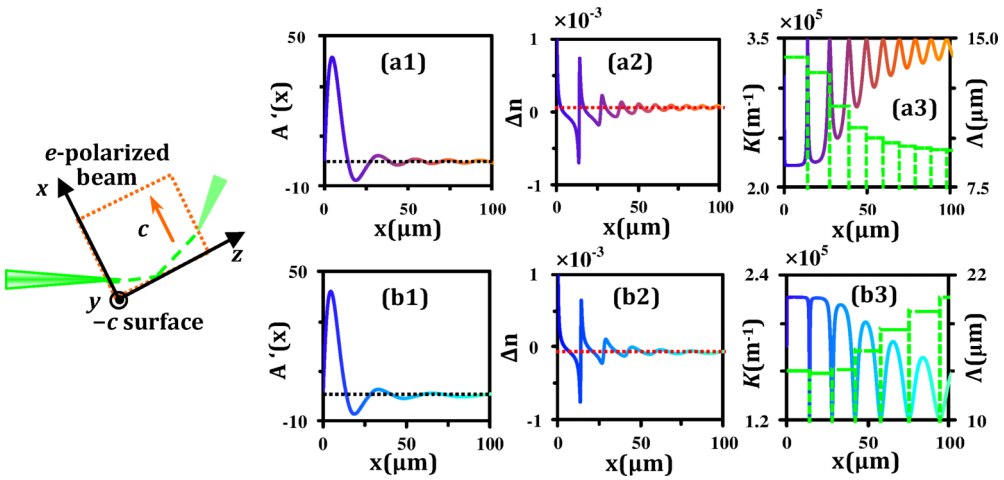

FIG. 1. (a1) and (b1) The PR SWs modes with $E_0 = -10^4$ and $10^4\,\text{V/m}$, respectively. (a2) and (b2) The distributions of refractive-index change corresponding to (a1) and (b1), respectively. (a3) and (b3) The distributions of the local spatial frequency $K(x)$ of PR SWs corresponding to (a1) and (b1) and the distributions of the channel width Λ_i corresponding to (a2) and (b2), respectively.

The modes of PR SWs are determined by the propagation constant and an external electric field. Figures 1(a1) and 1(b1) show the stationary PR SWs solutions with different $E_0 = -10^4$ and 10^4 V/m, respectively. From Eq. (6), the distributions of refractive-index change corresponding to the PR SWs in Figs. 1(a1) and 1(b1) are sketched in Figs. 1(a2) and 1(b2), respectively. The black dotted lines in the Figs. 1(a1) and 1(b1) and the red dotted lines in Figs. 1(a2) and 1(b2) represent the zero-level lines and the steady value at infinity, respectively. When these structures are fixed by the photofixation and electrofixation method, or directly guide weaker light or other light insensitive to the PR materials, the interesting photorefractive surface nonlinearly chirped waveguide arrays with apodized envelopes are induced. The first two channels still retain the abrupt characteristic which ensures the existence of extraordinary BGMs.

The width of each guided wave layer or channel of PR SNCWGAs is defined as channel width Λ_i, where i is the order of the guided wave layer or channel. The channel width Λ_i corresponding to Figs. 1(a2) and 1(b2) is shown as a green dotted histogram in Figs. 1(a3) and 1(b3). We can find that the Λ_i of PR SNCWGAs is characterized by a nonlinear chirp, besides the amplitude is apodized by the diffusion nonlinearity as Ref. [17]. The positive and negative chirp are determined by an external electric field, the Λ_i of the PR SNCWGAs with $E_0 = -10^4$ V/m [Fig. 1(a3)] and 10^4 V/m [Fig. 1(b3)] decrease (positive chirp) and increase (negative chirp), respectively. It is the result of the nearly saturated drift nonlinearity, and the saturation level can be fine tuned by a background beam. It is worth noting that the Λ of the second channel in Fig. 1(b3) slightly decreases owing to the cooperation diffusion nonlinearity and the damped amplitude of PR SWs. All the above phenomena can be understood clearly from Eq. (5), in that the channel width Λ decreases with the increase of the average frequency of PR SWs in each channel and vice versa, the analytic local spatial frequencies $K(x)$ of PR SWs are shown as the gradient solid lines in Figs. 1(a3) and 1(b3). Moreover, we can find that the PR SNCWGAs have a apodized tail converging to $n - \frac{1}{2}n^3 r_{\text{eff}} E_0$ which can be handily adjusted by an external electric field from Eq. (6), as shown in Figs. 1(a2) and 1(b2). That is very different from the case of only considering the diffusion nonlinearity, where the tail fixedly converges to 0.

III. THE REGULATION OF THE NONLINEAR CHIRP STRUCTURE

As is well known, PR SWs can be adjusted by an external electric field, background illumination, incident beam, etc. [18], so that we can expect that the nonlinear chirp structures of PR SNCWGAs can be regulated conveniently.

A. The condition for stable bright surface waves solutions

When an external electric field is applied to the SBN crystal, effective restoring force F and local spatial frequency $K(x)$ can be described by Eqs. (4) and (5), respectively. The equivalent force F as a function of amplitude $A'(x)$ is sketched in Fig. 2(a), and the influence of the external electric field on F can be analyzed for two cases: $a < g$ and $a > g$. When a low external electric field $E_0 < g/{k_0}^2 n^4 r_{\text{eff}}$ (i.e., $a < g$) is applied, F has only one point of intersection with the x axis at $A'(x) = 0$, which always exhibits an attractive force around $A'(x) = 0$ and corresponds to a stable balance position, as shown by the green dotted line in Fig. 2(a). The oscillation of PR SWs will converge at 0, corresponding to bright PR SWs. When a high external electric field $E_0 > g/{k_0}^2 n^4 r_{\text{eff}}$ (i.e., $a > g$) is applied, F has three points of intersection with the x axis at $A'_1(x) = 0$ and $A'_{2,3}(x) = \pm(a/g - 1)^{1/2}$, as shown by the red solid line in Fig. 2(a). F always exhibits repulsive force around $A'_1(x)$ while F always exhibits attractive force around $A'_{2,3}(x)$, thus $A'_1(x)$ is not an equilibrium position while $A'_{2,3}(x)$ are two nonzero equilibrium positions. As a result, $A'(x)$ does not converge at $A'_1(x)$=0 but converges at the couple of nonzero values $A'_{2,3}(x)$ at $x \to \infty$. It is inconsistent with the precondition $I'_\infty = I'(x \to \infty) = 0$ for a bright surface wave. Thus there is no stable bright surface wave solution when a higher external electric field is applied to the SBN crystal, that is, the applied external electric field has a threshold as $E_{\text{th}} = g/{k_0}^2 n^4 r_{\text{eff}}$, above which the bright surface wave cannot exist steadily. Obviously E_{th} is mainly determined by propagation constant β for a certain material, which is sketched in the red oblique line in Fig. 2(b). The green dotted line corresponds to $\beta = 2.730118 \times 10^7$ m^{-1} and the corresponding threshold electric field $E_{\text{th}} = 12781$ V/m. It should be noted that the distribution of E_{th} to β/nk_0 behaves as a parabola, we select only a narrow range of β/nk_0 so that the parabola looks like a line.

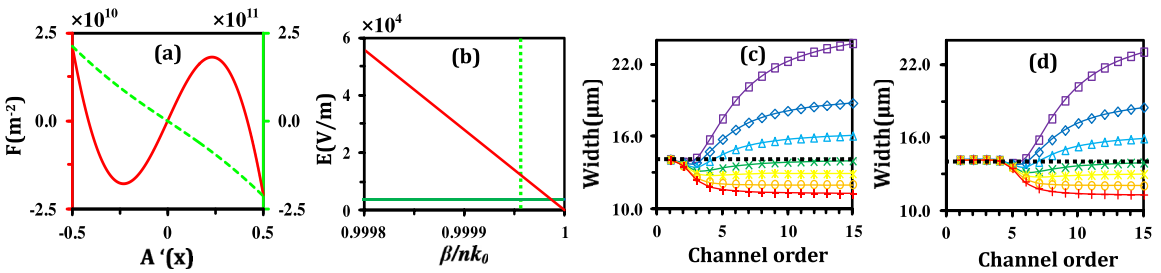

FIG. 2. (a) Effective restoring force F as a function of normalized amplitude $A'(x)$: solid and dotted curves correspond to $E_0 = 15\,000$ V/m ($a > g$) and 5000 V/m ($a < g$), respectively; (b) threshold electric field E_{th} (red oblique line) and critical electric field E_c (green solid line) as a function of propagation constant β/nk_0, respectively, the green dotted line correspond to $\beta = 2.730118 \times 10^7$ m^{-1}; (c) and (d) the distribution of channel width Λ_i to channel order i for the PR SNCWGAs induced by the PR SWs with $E_0 = -2000$, 0, 2000, 3574, 6000, 8000, and 10 000 V/m from bottom to top for lower $I'(x)$ and higher $I'(x) \sim 10^5$, respectively.

B. The regulation of the nonlinear chirp structure

The amplitude of PR SWs shows an oscillatory decay form from surface to bulk. Generally speaking, in the head region that is near the surface, the amplitude $A(x)$ of PR SWs is much larger than $I_d + I_b$ [i.e., $A'(x) \gg 1$], so that the period of PR SNCWGAs can be approximately written as $\Lambda_h = \pi/\sqrt{g - \gamma^2/4}$. In the tail region, the amplitude $A(x)$ of PR SWs approaches zero, so that the period of PR SNCWGAs can be approximately written as $\Lambda_t = \pi/\sqrt{g - a}$. Obviously the applied external electric field has a critical value as $E_c = \gamma^2/(4{k_0}^2 n^4 r_{\text{eff}})$, at which the period in the head region and tail region of PR SNCWGAs is equal (i.e., $\Lambda_h = \Lambda_t$). It means that the chirp of PR SNCWGAs can be suppressed to a minimum. E_c is not dependent on the propagation constant and it is equal to 3574 V/m under the conditions mentioned above, which is shown in the green solid line in Fig. 2(b). For a grazing angle approaching $\pi/2$ (i.e., $\beta/nk_0 \to 1$), there is no critical electric field E_c at which the chirp can be suppressed since there the E_c exceeds the threshold electric field E_{th}.

For convenience, we adopt the relation between channel width and channel order to describe the chirp structures of PR SNCWGAs. The chirp structures of the PR SNCWGAs induced by the PR SWs with $E_0 = -2000$, 0, 2000, 3574, 6000, 8000, and 10 000 V/m are orderly sketched in Fig. 2(c) from bottom to top, respectively. It is observed that the chirp parameters such as amplitude and sign (positive or negative) of PR SNCWGAs can be adjusted by an external electric field; the chirp of PR SNCWGAs is suppressed to a minimum at $E = E_c = 3574$ V/m, which is consistent with the theoretical analysis above. Moreover, the chirp structures can also be adjusted by background illumination and incident beam. Then we consider the situation for a much larger normalized intensity $I'(x)$, which can be adjusted by the intensity of background illumination and incident beam. Similarly, the chirp structures of PR SNCWGAs at $E_0 = -2000$, 0, 2000, 3574, 6000, 8000, and 10 000 V/m are orderly sketched in Fig. 2(d) from bottom to top. Compared with Fig. 2(c), the initial position of chirp goes away from the surface and the channels near the surface are characterized by fixed periodicity. From Eq. (5), the emergence of the chirp for PR SNCWGAs is essentially due to the normalized real amplitude $A'(x)$ of PR SWs is comparable to 1 so that the local spatial frequency $K(x)$ of PR SWs is modulated by $A'(x)$. In consequence, with the increase of $I'(x)$, the initial position of the chirp moves to the bulk along with the decaying of $A'(x)$.

IV. GUIDED WAVES

How do the nonlinear chirp and flexible tail influence the guided-wave properties of such intriguing waveguides? We then adopt the transfer matrix method to analyze the guided-wave properties of such interesting PR SNCWGAs, taking the TE modes for example. Considering a probe beam propagating in the PR SNCWGAs, the amplitude of TE modes satisfies

$$\frac{\partial^2 E_y(x)}{\partial x^2} + \left[k_0^2 n^2(x) - \beta^2\right] E_y(x) = 0, \tag{7}$$

where $E_y(x)$ is transverse electric polarized along the y direction, $n(x) = n + \Delta n(x)$.

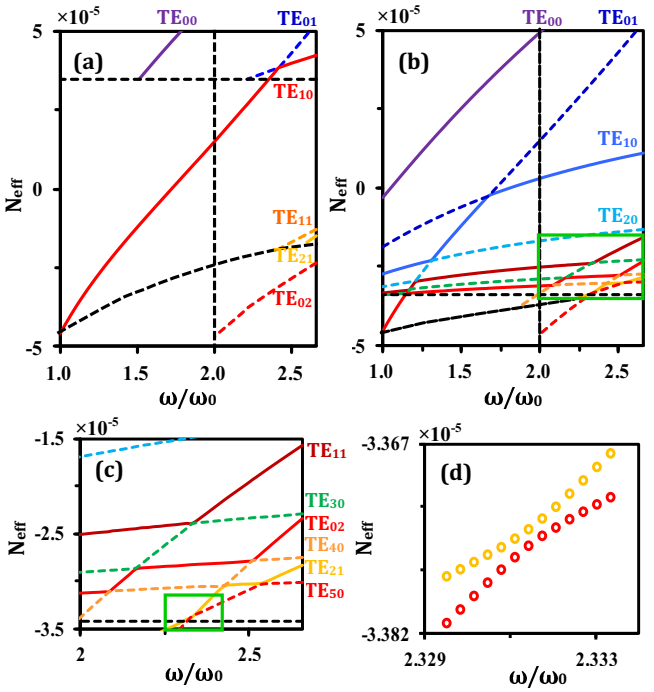

FIG. 3. (a) and (b) Dispersion relation of the PR SNCWGAs corresponding to PR SWs with $E_0 = -10^4$ and 10^4 V/m, respectively, the horizontal dotted line corresponds to $N_{\text{eff}} = -n^2 r_{\text{eff}} E_0/2$; (c) the fine structure of the green box in the (b); (d) the scatterplot of the anticrossing between the dispersion curves of TE_{21} and TE_{02}, corresponding to the green box in (c); and $N_{\text{eff}} = \beta/nk_0 - 1$ is the normalized effective refractive index.

We depict the dispersion relation corresponding to Figs. 1(a2) and 1(b2) in Figs. 3(a) and 3(b), respectively, Fig. 3(c) shows the fine structure of the green box in Fig. 3(b). $N_{\text{eff}} = \beta/nk_0 - 1$ is the normalized effective refractive index and ω/ω_0 is the normalized optical frequency, where ω_0 is the optical frequency of induction light. For convenience, the modes are designated as TE_{mn} with m as the mode index and n as the bound mechanism index, where $n = 0$, 1, 2 stand for IGMs, first BGMs, and second BGMs, respectively; furthermore, we label the dispersion curve of each mode by the accordant color along the border in Figs. 3(a)–3(c). As shown in Figs. 3(a)–3(c), the dispersion curves of IGMs and BGMs couple, intertwine, and anticross with each other, so that the dispersion curves of some modes are broken into many segments along the original curves. Moreover, the normalized mode for $\omega/\omega_0 = 2.66$ with $E_0 = 10^4$ V/m [the right edge of graph border in Figs. 3(b) and 3(c)] are orderly plotted in Figs. 4(a)–4(f) by using the same color as the corresponding dispersion curves, except the high order ($m \geqslant 2$) IGMs. Consistent with Ref. [17], the TE_{10} experienced anticrossing has an additional node, as shown in Fig. 4(c); there are two extraordinary BGMs (TE_{11} and TE_{21}) constituted by the splice of index-guided modes and Bragg-guided modes, as shown in Figs. 4(d) and 4(f), whose boundaries (the green dotted line) are located at $x = 14.09$ and 27.98 μm, corresponding to the first to second boundaries of PR SNCWGAs from surface to bulk, respectively.

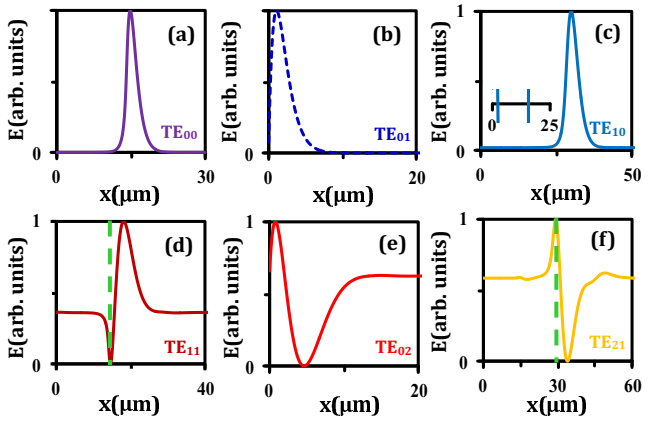

FIG. 4. The modes for $\omega/\omega_0 = 2.66$. (a)–(f) Correspond to intersections of dispersion curves and the right edge of picture box in Figs. 3(b) and 3(c) from top to bottom except the high order ($m \geqslant 2$) index-guided modes, respectively. Index-guided modes: (a) TE_{00} with $N_{\text{eff}} = 7.611\times10^{-5}$; (c) TE_{10} with $N_{\text{eff}} = 1.088\times10^{-5}$. First Bragg-guided modes: (b) TE_{01} with $N_{\text{eff}} = 5.228\times10^{-5}$; (d) TE_{11} with $N_{\text{eff}} = -1.571\times10^{-5}$; (f) TE_{21} with $N_{\text{eff}} = -2.840\times10^{-5}$. Second Bragg-guided modes: (e) TE_{02} with $N_{\text{eff}} = -2.338\times10^{-5}$.

A. Tailored dispersion curves of index-guided modes

Besides the anticrossing and extraordinary BGMs mentioned above, we have found lots of other intriguing phenomena in the PR SNCWGAs. First, compared with the dispersion relation with $E_0 = -10^4$ V/m shown in Fig. 3(a), the dispersion relation with $E_0 = 10^4$ V/m shown in Fig. 3(b) has more intertwined structure, which relates to the sharply declined number of IGMs with $E_0 = -10^4$ V/m. This drastic change is the result of the apodized tail converging to $n - \frac{1}{2}n^3 r_{\text{eff}} E_0$, as depicted in Figs. 1(a2) and 1(b2). Considering the quasiperiodic layered structures of PR SNCWGAs, we can clearly understand such guided wave problems by using the classical concept of multichannel waveguides.

Physically the multichannel waveguide can be considered as a system of N interacting slab waveguides. Each confined mode of the single slab waveguide will gives rise to N nondegenerate modes as a result of the interacting between the different channels [26]. For the PR SNCWGAs induced by PR SWs, only fundamental IGMs can be excited owing to the rather low modulation depth of the refractive-index change, the numerous IGMs are the result of the fundamental mode splitting. In consequence, the number of IGMs is equal to the number of effective channels which are strong enough to split a new mode through the interaction between channels. Whether the channel is effective depends on the modulation depth of each channel, that is, the difference of refractive-index between each guided wave layer and substrate. The waveguide arrays induced by PR SWs take the air and the crystal self as the cladding and substrate layers, respectively. Owing to the drift nonlinearity, the PR SNCWGAs have a tunable tail converging to $n - \frac{1}{2}n^3 r_{\text{eff}} E_0$, that is, the refractive-index of the substrate layer can be adjusted by an external electric field. Compared with the PR SNCWGA with $E_0 = 10^4$ V/m, the PR SNCWGA with $E_0 = -10^4$ V/m has a distinctly higher substrate refractive index so that it has less effective channels and IGMs. This implies that the dispersion curves of the IGMs can be tailored by an external electric field, which can help to control the modes excitation conveniently.

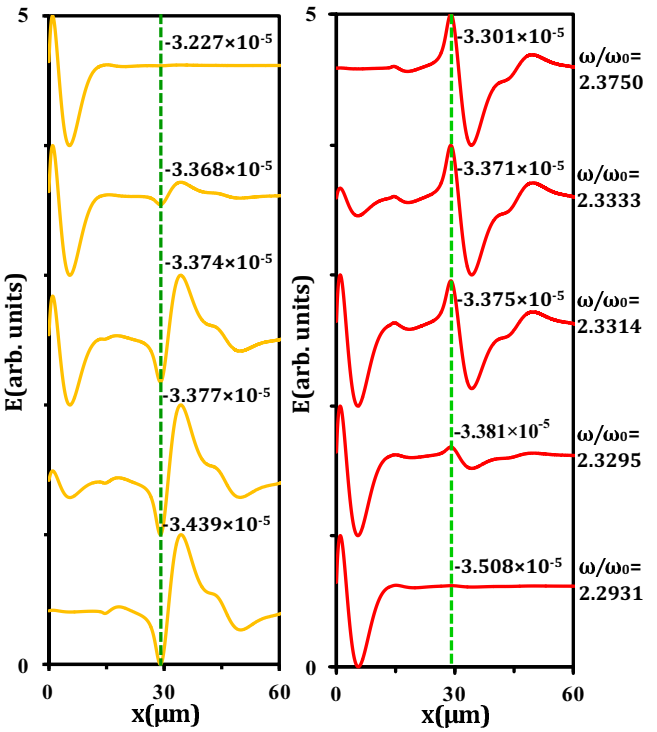

FIG. 5. The mode evolution of each dispersion branch associated with the anticrossing between TE_{21} and TE_{02}. Left-hand side: The modes evolution from TE_{21} to TE_{02} corresponding to the upper and lower branch in Fig. 3(d). Right-hand side: The modes evolution from TE_{02} to TE_{21} corresponding to the lower branch in Fig. 3(d). The green dotted lines show the boundary of IGM region and BGM region for TE_{21}.

B. The anticrossing between ordinary and extraordinary Bragg guided modes

In general, the interesting phenomenon that the dispersion curves couple, intertwine, and anticross with each other happens where IGMs and BGMs intersect. However, we are surprised to find that there is an identical anticrossing phenomenon between the extraordinary BGMs TE_{21} and the ordinary BGMs TE_{02}, as shown in the green box of Fig. 3(c). Figure 3(d) shows the local scatter plot of the anticrossing between TE_{21} and TE_{02}, and the scatter points are plotted in the same color as the corresponding dispersion curves.

Meanwhile, in order to present the details of anticrossing phenomenon between TE_{21} and TE_{02}, the mode evolution of each dispersion branch associated with such anticrossing are sketched in Fig. 5, the green dotted lines show the second boundary of PR SNCWGAs from surface to bulk, which is also the boundary of IGM region and BGM region for TE_{21}. The left-hand side and right-hand side show the evolution of the modes corresponding to the upper and lower branches, respectively, and the upper branch stands for the evolution from TE_{21} to TE_{02}, and the lower branch stands for the evolution

from TE_{02} to TE_{21}. The modes for $\omega/\omega_0 = 2.2931$, 2.3750 stand for the situation before and after such anticrossing and the modes for $\omega/\omega_0 = 2.3295$, 2.3314, and 2.3333 stand for the situation near such anticrossing. Obviously there is a clear "competition" between the TE_{21} and TE_{02} in the coupling hybrid modes near anticrossing, which further display the detail of coupling and anticrossing between the TE_{21} and TE_{02}. Compared with the TE_{21} for $\omega/\omega_0 = 2.2931$, the TE_{21} for $\omega/\omega_0 = 2.3750$, which has experienced an anticrossing, has an additional node in the left side of the boundary where the mode presents the characteristic of IGMs. Such anticrossing is due to the nonlinear chirp modulation of PR SNCWGAs. In the PR SNCWGAs, the first two channel boundaries can be regarded as abrupt interfaces, and the right region of boundary can be seen as a new PR SNCWGA profile, the self-similarity between the new and the original PR SNCWGA is broken owing to the nonlinear chirp. Thus the dispersion curves of TE_{02} and TE_{21} are no longer like AWGAs in which these two dispersion curves evolve almost parallel along the optical frequency, and such nonparallel evolution of dispersion curves provides the possibility for anticrossing.

As is well known, the anticrossing opens up a mini gap or mode gap in the dispersion relation and thus gives rise to a mini stop band (MSB) in the transmission spectrum of the corresponding mode [27]. Moreover, the MSBs have vast potential applications in filter, sensor, group velocity modulation or control, broadband switching and spectrometry, etc. [28–32]. Owing to chirp, the MSBs can occur in the Bragg band gap for the PR SNCWGAs, compared with the AWGAs; meanwhile, the extraordinary BGMs localize the probe wave within the confined layer. Such more abundant anticrossings will have a greater prospect.

V. CONCLUSIONS

In summary, we have reported an alternate type of nonlinear waveguides, nonlinearly chirped waveguide arrays with apodized envelopes, induced by PR SWs in virtue of the diffusion and drift nonlinearities. Subsequently, we have studied the regulation of the nonlinear chirp structure and found that the chirp parameters such as amplitude, sign (positive or negative), and initial position can be adjusted conveniently. Finally, we have analyzed the guided-wave properties of such waveguide arrays. The PR SNCWGAs are of many interesting guided-wave properties, such as the dispersion relation of IGMs tailored by an external electric field which can help to control modes excitation and the anticrossing between the ordinary and extraordinary BGMs which provides more abundant anticrossings or mini gaps. The amplitude or/and frequency modulation of waveguide arrays provide new opportunities for soliton control, diffraction management, quasi-phase-matched and optical diode, etc. The MSBs arising from anticrossing have vast potential applications in filter, sensor, group velocity modulating or controlling, broadband switching and spectrometry, etc. Moreover, owing to its convenience in fixing, scrubbing, adjusting, and controlling, the PR SNCWGAs have a great prospect for the developments and applications of integrated optical components and optoelectronic devices.

ACKNOWLEDGMENTS

This work is supported by the Chinese National Key Basic Research Special Fund (2011CB922003), National Natural Science Foundation of China (61178005, J1103208), and Specialized Research Fund for the Doctoral Program of Higher Education (20120031110030).

[1] D. N. Christodoulides, F. Lederer, and Y. Silberberg, Nature (London) **424**, 817 (2003).
[2] J. M. Lourtioz, H. Benisty, V. Berger, J. M. Gerard, D. Maystre, and A. Tchelnokov, *Photonic Crystals: Towards Nanoscale Photonic Devices* (Springer, Berlin, 2005).
[3] N. K. Efremidis, S. Sears, D. N. Christodoulides, J. W. Fleischer, and M. Segev, Phys. Rev. E **66**, 046602 (2002).
[4] J. W. Fleischer, T. Carmon, M. Segev, N. K. Efremidis, and D. N. Christodoulides, Phys. Rev. Lett. **90**, 023902 (2003).
[5] J. W. Fleischer, M. Segev, N. K. Efremidis, and D. N. Christodoulides, Nature (London) **422**, 147 (2003).
[6] B. Freedman, G. Bartal, M. Segev, R. Lifshitz, D. N. Christodoulides, and J. W. Fleischer, Nature (London) **440**, 1166 (2006).
[7] O. Peleg, G. Bartal, B. Freedman, O. Manela, M. Segev, and D. N. Christodoulides, Phys. Rev. Lett. **98**, 103901 (2007).
[8] J. Xavier, M. Boguslawski, P. Rose, J. Joseph, and C. Denz, Adv. Mater. **22**, 356 (2010).
[9] M. Segev, Y. Silberberg, and D. N. Christodoulides, Nat. Photon. **7**, 197 (2013).
[10] C. R. Rosberg, I. L. Garanovich, A. A. Sukhorukov, D. N. Neshev, W. Krolikowski, and Y. S. Kivshar, Opt. Lett. **31**, 1498 (2006).
[11] A. A. Sukhorukov, Phys. Rev. Lett. **96**, 113902 (2006).
[12] E. Smirnov, C.E. Rüter, D. Kip, K. Shandarova and V. Shandarov, Appl. Phys. B **88**, 359 (2007).
[13] G. S. Garcia Quirino, J. J. Sanchez-Mondragon, and S. Stepanov, Phys. Rev. A **51**, 1571 (1995).
[14] I. I. Smolyaninov, C. H. Lee, and C. C. Davis, Phys. Rev. Lett. **83**, 2429 (1999).
[15] T. H. Zhang, J. Yang, H. Z. Kang, L. Feng, J. J. Xu, C. P Zhang, X. K. Ren, B. H. Wang, Y. Z. Lu, F. Jia, and W. W. Shao, Phys. Rev. B **73**, 153402 (2006).
[16] W. W. Shao, L. Li, W. W. Liu, T. H. Zhang, H. H. Ma, J. J. Xu, and J. G. Tian, Appl. Phys. Lett. **95**, 211105 (2009).
[17] P. F. Qi, Z. J. Hu, R. Han, T. H. Zhang, J. G. Tian, and J. J. Xu, Opt. Express. **23**, 31144 (2015).
[18] T. H. Zhang, X. K. Ren, B. H. Wang, C. B. Lou, Z. J. Hu, W. W. Shao, Y. H. Xu, H. Z. Kang, J. Yang, D. P. Yang, L. Feng, and J. J. Xu, Phys. Rev. A **76**, 013827 (2007).
[19] A. Szameit, Y. V. Kartashov, F. Dreisow, M. Heinrich, T. Pertsch, S. Nolte, A. Tünnermann, V. A. Vysloukh, and L. Torner, Opt. Lett. **33**, 1132 (2008).
[20] G. Y. Yin, J. B. Zheng, and L. W. Dong, Opt. Commun. **283**, 583 (2010).

[21] B. Zheng, C. G. Huang, S. S. Zhong, and L. W. Dong, J. Opt. Soc. Am. B. **27**, 2224 (2010).
[22] C. Y. Li, R. Cui, F. W. Ye, Y. V. Kartashov, L. Torner, and X. F. Chen, Opt. Lett. **40**, 898 (2015).
[23] L. Gu, D. C. Guo, and L. W. Dong, Opt. Express. **23**, 12434 (2015).
[24] B. Q. Chen, C. Zhang, C. Y. Hu, R. J. Liu, and Z. Y. Li, Phys. Rev. Lett. **115**, 083902 (2015).
[25] H. J. Li, Z. G. Deng, J. S. Huang, S. H. Fu, and Y. Y. Li, Opt. Lett. **40**, 2572 (2015).
[26] P. Yeh, A. Yariv, and C. S. Hong, J. Opt. Soc. Am. **67**, 423 (1977).
[27] S. Olivier, M. Rattier, H. Benisty, C. Weisbuch, C. J. M. Smith, R. M. De La Rue, T. F. Krauss, U. Oesterle, and R. Houdré, Phys. Rev. B **63**, 113311 (2001).
[28] A. Y. Petrov and M. Eich, Appl. Phys. Lett. **85**, 4866 (2004).
[29] N. Shahid, N. Speijcken, S. Naureen, M. Y. Li, M. Swillo, and S. Anand, Appl. Phys. Lett. **98**, 081112 (2011).
[30] Y. Cui, X. Feng, Y. D. Huang, Q. Zhao, Z. L. Huang, and W. Zhang, Appl. Phys. Lett. **101**, 151110 (2012).
[31] N. Shahid, M. Amin, S. Naureen, and S. Anand, AIP Adv. **3**, 032136 (2013).
[32] M. G. Scullion, A. Di Falco, and T. F. Krauss, Opt. Lett. **39**, 4345 (2014).